npj | precision oncology

Article

Published in partnership with The Hormel Institute, University of Minnesota

https://doi.org/10.1038/s41698-025-00966-x

Machine learning-based MRI radiomics predict IL18 expression and overall survival of low-grade glioma patients

Zhe Zhang[1,2,3,4,5], Yao Xiao[1,2,3,4,5], Jun Liu[1,2,3,4,5], Feng Xiao[1,2,3,4], Jie Zeng[1,2,3,4], Hong Zhu[1,2,3,4] ✉, Wei Tu[1,2,3,4] ✉ & Hua Guo[1,2,3,4] ✉

Interleukin-18 has broad immune regulatory functions. Genomic data and enhanced Magnetic Resonance Imaging data related to LGG patients were downloaded from The Cancer Genome Atlas and Cancer Imaging Archive, and the constructed model was externally validated using hospital MRI enhanced images and clinical pathological features. Radiomic feature extraction was performed using "PyRadiomics", feature selection was conducted using Maximum Relevance Minimum Redundancy and Recursive Feature Elimination methods, and a model was built using the Gradient Boosting Machine algorithm to predict the expression status of IL18. The constructed radiomics model achieved areas under the receiver operating characteristic curve of 0.861, 0.788, and 0.762 in the TCIA training dataset (n = 98), TCIA validation dataset (n = 41), and external validation dataset (n = 50). Calibration curves and decision curve analysis demonstrated the calibration and high clinical utility of the model. The radiomics model based on enhanced MRI can effectively predict the expression status of IL18 and the prognosis of LGG.

Primary central nervous system (CNS) tumors are attributed to ~250,000 deaths annually because treatment was very difficult[1]. Gliomas are the most common primary CNS tumors, including various types such as astrocytomas, oligodendrogliomas, ependymomas, and malignant glioblastomas[2]. According to the latest classification of central nervous system tumors released by the World Health Organization (WHO) in 2016, tumors categorized as Grade II and Grade III based on histopathology are classified as low-grade gliomas (LGG)[3,4]. In recent years, significant progress has been made in the diagnosis and treatment of LGG. However, LGG inevitably undergoes tumor recurrence and malignant progression after initial treatment, significantly affecting the quality of life of these patients[5]. Due to challenges such as the blood-brain barrier, many challenging issues remain, necessitating further research exploration and clinical practice to seek more effective and timely diagnosis and treatment.

Interleukin-1 (IL-1) is the first discovered interleukin and a central mediator of innate immunity and inflammation[6]. Interleukin-18 (IL18) is a multifunctional cytokine that belongs to the pro-inflammatory cytokines of the IL-1 family[7,8]. IL18 is primarily secreted by liver Kupffer cells and macrophages, promoting NK cell activity and T cell proliferation, participating in the regulation of inflammation, cell apoptosis, immune cell activation, and other immune responses, playing an important role in the immune system[9]. Additionally, IL18 has been found to be associated with the development and progression of various diseases, including inflammatory diseases, autoimmune diseases, and tumors[10]. IL18 can promote the secretion of Th1-type cytokines, stimulate NK cells and T cells to secrete IFNγ, induce the production of cytokines such as GM-CSF, TNF-α, IL-1β, thereby promoting anti-tumor immune responses[11,12]. At present, there have been significant breakthroughs in IL18 immunotherapy. IL18's involvement in immune regulation makes it an important target for disease treatment research. Small molecule drugs targeting IL18 have shown good efficacy in tumor treatment[11]. However, traditional IL18 detection methods, including peripheral blood tests, fresh tissue specimen mRNA or protein level tests, and paraffin-embedded tissue specimen tests, have disadvantages such as high costs and susceptibility to operator and antibody influence. Currently, there is still a lack of noninvasive and dynamically monitorable methods for IL18 in LGG, which may limit the ability to identify IL18 treatment-sensitive populations.

Brain magnetic resonance imaging (MRI) is commonly used to examine and assess various brain diseases, as it can accurately display the extent of diffusion and depth of infiltration of gliomas[13]. Compared to other

[1]Department of Neurosurgery, The Second Affiliated Hospital, Jiangxi Medical College, Nanchang University, Nanchang, China. [2]Institute of Neuroscience, Nanchang University, Jiangxi, China. [3]Jiangxi Province Key Laboratory of Neurological Diseases, Jiangxi, China. [4]JXHC Key Laboratory of Neurological medicine, Jiangxi, China. [5]These authors contributed equally: Zhe Zhang, Yao Xiao, Jun Liu. ✉e-mail: zhuzuhongzhuzuhong@outlook.com; tw200609@163.com; ndefy02014@ncu.edu.cn

Table 1 | Patient clinical characteristics

Variables	Total (n = 461)	Low (n = 314)	High (n = 147)	p
Age, n (%)				0.748
~40	223 (48)	154 (49)	69 (47)	
41~	238 (52)	160 (51)	78 (53)	
Gender, n (%)				0.977
Female	209 (45)	143 (46)	66 (45)	
Male	252 (55)	171 (54)	81 (55)	
Histologic_grade, n (%)				<0.001
G2	224 (49)	171 (54)	53 (36)	
G3	237 (51)	143 (46)	94 (64)	
Radiotherapy, n (%)				<0.001
NO	198 (43)	156 (50)	42 (29)	
YES	263 (57)	158 (50)	105 (71)	
Histological_type, n (%)				<0.001
Astrocytoma	174 (38)	84 (27)	90 (61)	
Oligoastrocytoma	121 (26)	88 (28)	33 (22)	
Oligodendroglioma	166 (36)	142 (45)	24 (16)	
Chr_1p_19q_codeletion, n (%)				< 0.001
Non-Codel	310 (67)	171 (54)	139 (95)	
Codel	151 (33)	143 (46)	8 (5)	
IDH_status, n (%)				< 0.001
WT	84 (18)	37 (12)	47 (32)	
Mutant	377 (82)	277 (88)	100 (68)	
MGMT_promoter_status, n (%)				<0.001
Unmethylated	81 (18)	37 (12)	44 (30)	
Methylated	380 (82)	277 (88)	103 (70)	
Chemotherapy, n (%)				0.004
NO	194 (42)	147 (47)	47 (32)	
YES	267 (58)	167 (53)	100 (68)	

methods, brain MRI is the most accessible and direct examination method for clinical diagnosis of the nervous system[14]. In recent years, with the continuous development of artificial intelligence, machine learning radiomics analysis has played an increasingly important role in tumor research[15–17]. Clinicians can extract various features from brain MRI to more accurately diagnose diseases, stage them, and predict patient prognosis, thereby formulating personalized treatment plans[18–20]. Therefore, this study explored the potential molecular mechanisms of IL18 expression and its association with the immune microenvironment through RNA and clinical data from TCGA. It also validated the correlation between IL18 and LGG in an external hospital cohort through RNA and immunohistochemistry. Furthermore, leveraging integrated clinical, transcriptomic, and imaging data from TCGA and TCIA, we have developed a novel noninvasive MRI-based radiomics machine learning framework to predict IL18 expression status and prognostic outcomes in low-grade glioma patients. Finally, external validation was performed through the hospital cohort, confirming the model's robustness.

Results

IL18 expression level, clinical characteristics, and prognosis analysis in low-grade gliomas

The research flowchart is shown in Fig. 1. Based on a cutoff value of 2.477 for IL18 expression, 461 cases of low-grade glioma patients in the TCGA database were divided into a high-expression group with 147 cases and a low-expression group with 314 cases. We found differences in the distribution of Histologic_grade, Histological_type, Chemotherapy, and Radiotherapy status between the high and low IL18 expression groups (P < 0.001, Table 1). Through analysis of low-grade glioma patient data in the TCGA database, we observed that IL18 was significantly upregulated in tumor tissues compared to non-tumor tissues (P = 0.04, Fig. 2A). Kaplan-Meier curves showed that patients with high IL18 expression had significantly lower overall survival (OS) than those with low IL18 expression (P < 0.001; Fig. 2B). In addition, Age, Histologic_grade, Histological_type, Chr_1p_19q_codeletion, IDH_status, MGMT_promoter_status, Chemotherapy, and Radiotherapy were also significantly associated with OS (Supplementary Fig. 1A-H). Further univariate Cox analysis showed that IL18, Age, Histologic_grade, and IDH_status were all high-risk factors (Fig. 2D), and multivariate Cox analysis showed that IL18 was an independent prognostic factor for LGG OS [hazard ratio (HR) 1.978, 95% CI 1.296–3.019; p = 0.002; Fig. 2D]. Subgroup analysis showed that IL18 and selected covariates did not interact (Supplementary Fig. 2). Moreover, IL18 expression was significantly associated with Histologic_grade, Radiotherapy, Histological_type, Chr_lp_19q_codeletion, MGMT promoter_status, and IDH_status (Fig. 2F). To further validate IL18 expression in low-grade gliomas, qRT-PCR analysis was performed on a cohort of patients from the Neurosurgery Center of the Second Affiliated Hospital of Nanchang University, revealing a significant upregulation of IL18 in low-grade glioma tissues compared to normal brain tissues (Fig. 2C). Immunohistochemistry (IHC) staining for IL18 expression showed significantly positive staining in LGG patients compared to normal brain tissues (Fig. 2E).

Mechanistic exploration of IL18 in low-grade gliomas

Analysis of glioma single-cell sequencing data revealed that IL18 was primarily expressed in Macrophage-C1QC-C3, Macrophage-C1QC-PLTP, and Macrophage-SPP1-ACP5 clusters among 11 immune cell clusters (Fig. 3A, B). Furthermore, the infiltration of immune cells in low-grade gliomas was further analyzed, showing significantly increased infiltration of T cells CD8, T cells CD4 memory resting, Monocytes, and Macrophages M2 in the high IL18 expression group (Fig. 3C). Through tumor microenvironment analysis, we found that the StromalScore, ImmuneScore, and EstimateSocre were all higher in the high IL18 expression group compared to the low IL18 expression group (Supplementary Fig. 3A). Analysis of the efficacy of immune checkpoint inhibitor therapy in LGG patients revealed that the number of immune therapy responders was significantly lower in the high IL18 expression group compared to the low expression group (Supplementary Fig. 3B). KEGG enrichment analysis showed significant enrichment mainly in the JAK/STAT (JAK_STAT_SIGNALING_PATHWAY), B_CELL_RECEPTOR_SIGNALING_PATHWAY, and Toll-like receptor (TOLL_LIKE_RECEPTOR_SIGNALING_PATHWAY) signaling pathways (Supplementary Fig. 3C). Hallmark enrichment analysis indicated significant enrichment of the KRAS (KRAS_SIGNALING) signaling pathway in the high-expression group of IL18 (Supplementary Fig. 3D).

IL18 in in vivo and in vitro experiments on gliomas

In the TCGA and CGGA databases, the expression of IL18 varies among different grades of gliomas, with its expression increasing as the malignancy of the tumor rises (Supplementary Fig. 4A, B). Additionally, Kaplan-Meier curves indicate that patients with high IL18 expression have significantly lower overall survival (OS) compared to those with low IL18 expression (p < 0.001; Supplementary Fig. 4C, D). To determine whether IL18 is involved in the malignant progression of gliomas, we conducted further cellular functional experiments. Colony formation assays showed that knocking out IL18 significantly reduced cell colonies compared to the NC group (Fig. 4A, B). In wound healing assays, we observed that reducing IL18 expression significantly hindered the migration of glioma cells (Fig. 4C, D). Through transwell experiments, we found that the invasion ability of U118MG and U251MG cells was weakened after IL18 knockout (Fig. 4E, F). Furthermore, to investigate whether IL18 knockout affects in vivo glioma growth, we established a tumor model in nude mice. The results showed that compared to the control group, the tumor volumes of mice in the sh-IL18#1

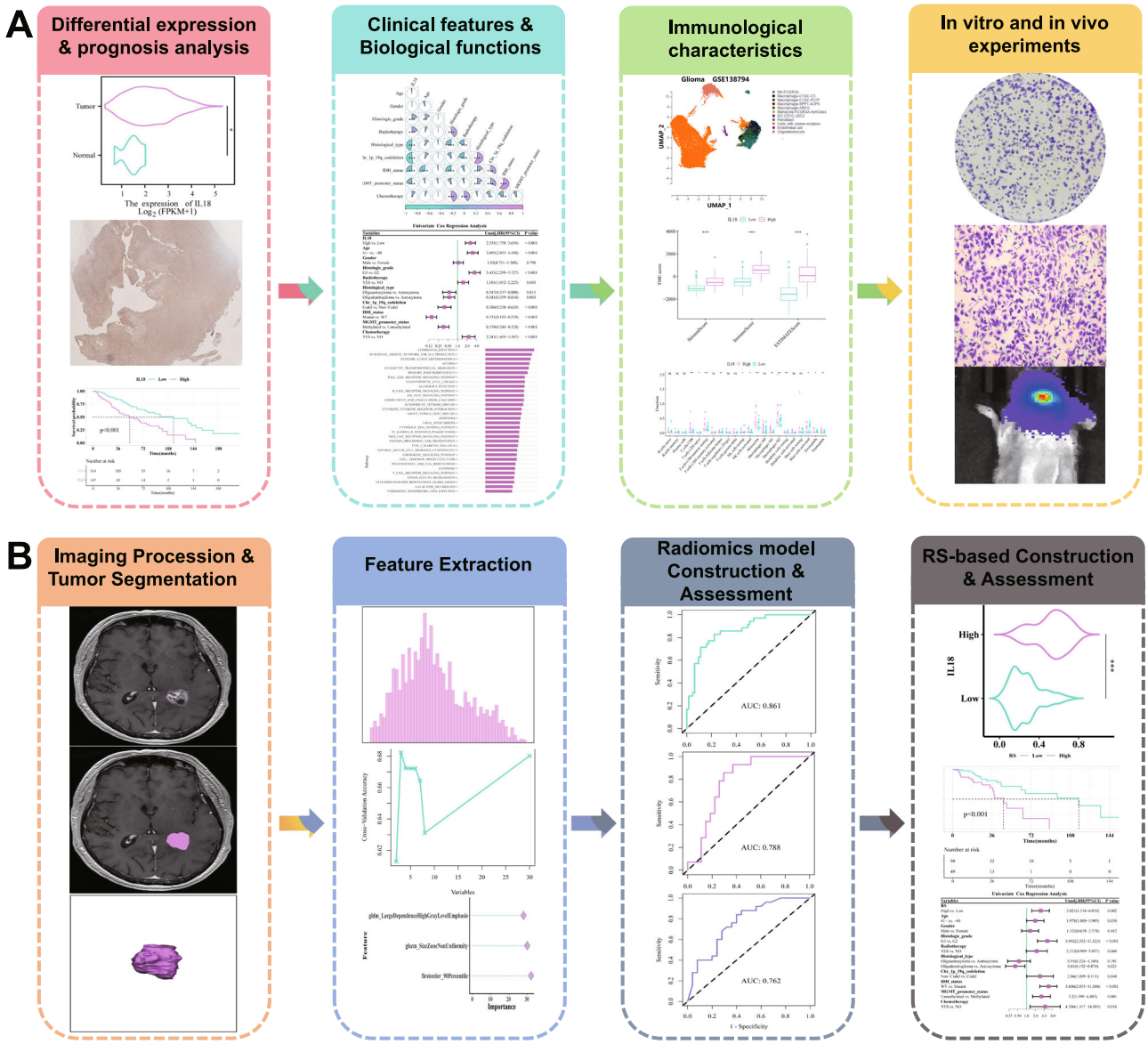

Fig. 1 | Schematic diagram of research content. A Expression and prognosis analysis, clinical characteristics, biological functions, and immunological characteristics. **B** Image processing and tumor segmentation, feature extraction, construction and evaluation of radiomics models, construction and evaluation of radiomics scores.

and sh-IL18#2 groups were significantly reduced (Fig. 5A), exhibiting weaker overall fluorescence intensity (Fig. 5B), slower weight loss (Fig. 5C), and longer overall survival time (Fig. 5D).

Radiomics feature extraction, model construction, and evaluation for predicting IL18

The TCGA and TCIA intersection dataset was randomly divided into a training set of 98 cases and a validation set of 41 cases. The p-values of the differential analysis between the two groups for Age, Gender, Histologic_grade, Radiotherapy, Histological_type, Chr_lp_19q_codeletion, IDH_status, MGMT_promoter_status, Chemotherapy, and IL18 were all >0.05 (Table 2). External validation was performed using a cohort of 50 cases from the Neurosurgery Center of the Second Affiliated Hospital of Nanchang University (Supplementary Table 1). The mRMR method and RFE method were used to select radiomic features, obtaining the best 3 features (Supplementary Fig. 5), with ICC values all above 0.75 (Supplementary Table 2). The constructed radiomic model underwent ROC curve and calibration curve analysis, with AUC values of 0.861 in the training set (Fig. 6A, D), 0.788 in the validation set (Fig. 6B, E), and 0.762 in the external validation set (Fig. 6C, F). DCA demonstrated that the model had high clinical utility (Fig. 6G–I).

Radiomics score assessment predicts the prognosis of patients with LGG

Based on the expression of the Radiomics score (Rad_score) with a cutoff value of 0.4416, it was divided into a high-expression group of 49 cases and a low-expression group of 90 cases, and a baseline data table of clinical variables was plotted. We found significant differences in Histologic_grade, Histological_type, Chr_1p_19q_codeletion, IDH_status, and MGMT_promoter_status between the high and low Rad_score groups (Supplementary Table 3). In the training set, validation set, and external validation set, there were significant differences in Rad_score between the high and low expression groups of IL18 ($p < 0.05$; Fig. 7A–C). Kaplan-Meier curves showed a significant correlation between high Rad_score and deteriorated OS (Fig. 7D), with a median survival time of 46.7 months in the high Rad_score group and 115.67 months in the low Rad_score group. Additionally, univariate analysis showed that Rad_score was a high-risk factor, and it was also

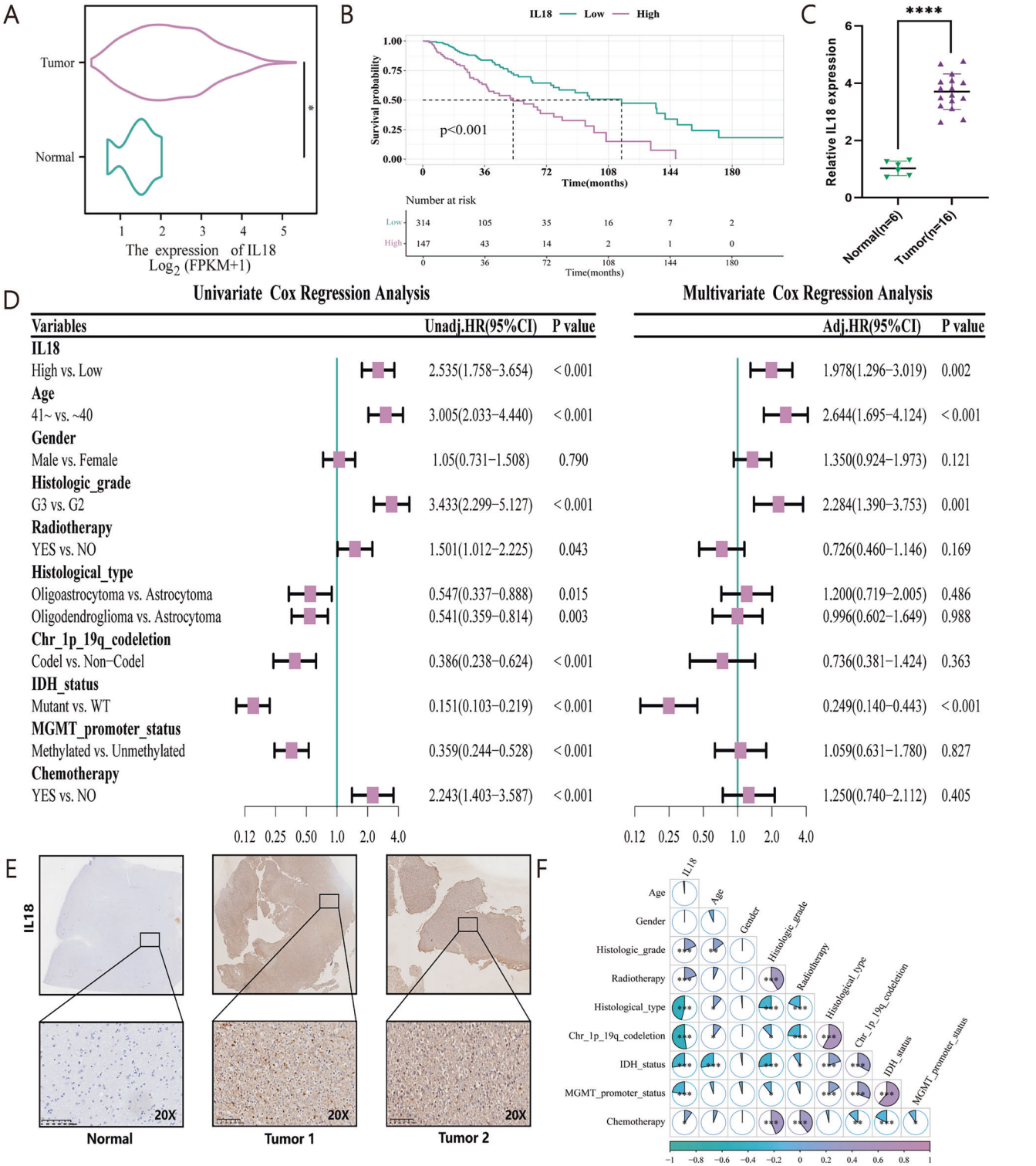

Fig. 2 | Correlation between IL18 expression level and clinical features. **A** IL18 is highly expressed in gliomas. **B** Kaplan-Meier curve shows a significant correlation between high expression of IL18 and deteriorated OS. **C** qRT-PCR analysis shows high expression of IL18 in low-grade glioma tissue. **D** Univariate and multivariate Cox regression analyses show that high expression of IL18 is an independent prognostic factor for OS. **E** IHC detection of IL18 expression. **F** Correlation analysis between IL18 and clinical features (*p < 0.05, **p < 0.01, ***p < 0.001).

found that Histologic_grade, IDH_status, MGMT_promoter_status, and Chemotherapy were risk factors for OS (Fig. 7E). Multivariate analysis showed that Rad_score was an independent prognostic factor for LGG OS [hazard ratio (HR) 2.723, 95% CI 1.219−6.080; p = 0.015; Fig. 7D]. Subgroup analysis showed that Rad_score and selected covariates had no interaction (Fig. 7F).

Discussion

Low-grade gliomas are characterized by high disability and mortality rates, with malignant transformation potential, often resulting in a median survival rate of less than 10 years[21]. Classic prognostic indicators for gliomas include clinical and pathological characteristics, IDH, MGMT, among others. However, these indicators no longer meet the clinical requirements

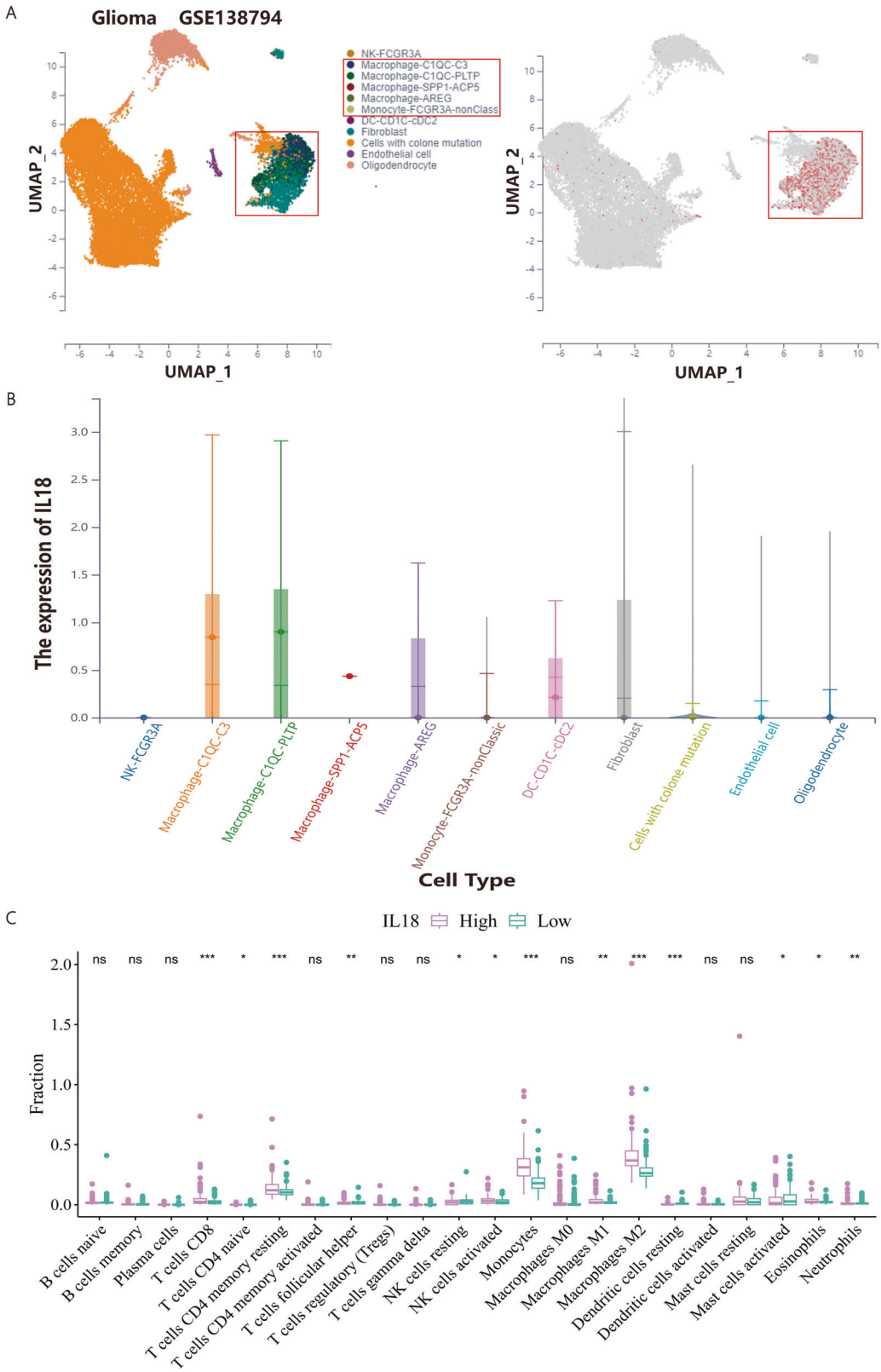

Fig. 3 | Analysis of IL18 and immune cell infiltration in low-grade gliomas. **A** Clustering analysis of 11 immune cells in glioma single-cell sequencing. **B** Expression and distribution of IL18 in 11 immune cells. **C** Immune cell infiltration (*p < 0.05, **p < 0.01, ***p < 0.001).

of precision medicine[22–25]. Exploring a technique that can noninvasively and dynamically detect and quantitatively respond to tumor characteristics for early diagnosis of low-grade gliomas, assessment of tumor heterogeneity, and improvement of treatment efficacy is urgently needed. In this study, we integrate and process transcriptome sequencing data and medical imaging data from the TCGA and TCIA databases, respectively. We utilize MRI-enhanced images and clinical pathological characteristics from the Neurosurgery Center of the Second Affiliated Hospital of Nanchang University for

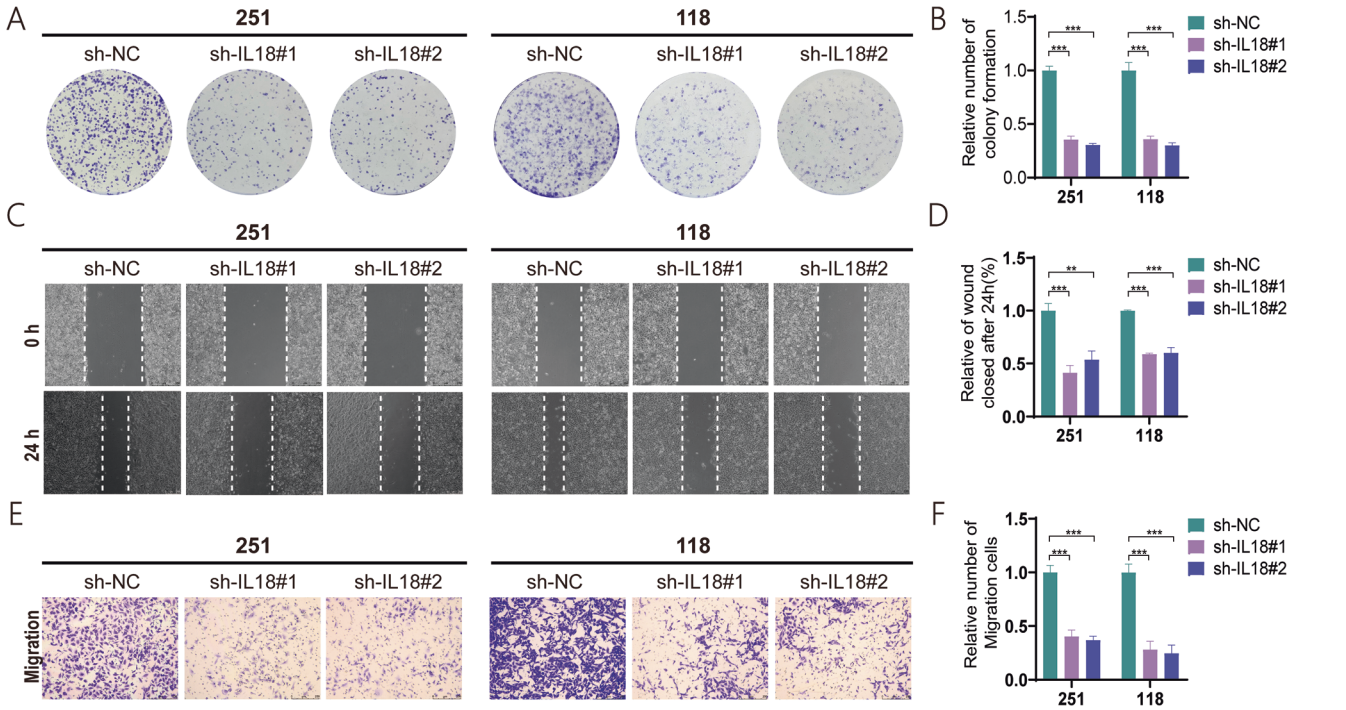

Fig. 4 | Knockout of IL18 inhibits proliferation, migration, and invasion of glioma cells. The effects of IL18 knockout on colony formation in U118MG and U251MG cells (**A**) and histogram analysis (**B**). The results of wound healing assays after IL18 knockout in U118MG and U251MG cells (**C**) and histogram analysis (**D**). The effects of IL18 knockout on Transwell assays in U118MG and U251MG cells (**E**) and histogram analysis (**F**) (*p < 0.05, **p < 0.01, ***p < 0.001).

external validation of the constructed model. We investigate the expression status and prognostic value of IL18, immune-related mechanisms, and the prognostic value of radiomics prediction models.

Natural killer (NK) cells, a critical component of the innate immune system, serve as key effectors of cytotoxic activity against infected or malignant cells[26]. In contrast, T cells, which constitute the cornerstone of the adaptive immune response, are responsible for antigen-specific recognition and targeted elimination of pathogens and aberrant cells[27]. IL18, a member of the IL-1 cytokine family, induces IFNγ production in NK cells and T cells, exhibiting broad immunomodulatory functions[28,29]. In this study, we found that compared to normal tissues, IL18 was highly expressed in gliomas, and patients with high IL18 expression had poorer overall survival (OS). Univariate and multivariate analyses revealed that IL18 expression was an independent prognostic factor for low-grade gliomas. In previous studies, Virginie et al. found a significant correlation between the pro-tumor effect of IL18 and its high expression in gastric tumor epithelium[30]. Anne et al. found significant expression of IL18 in unstable colorectal cancer, which was associated with high density of T lymphocytes[31]. Wang et al. found significant overexpression of IL18 in renal cell carcinoma (RCC) tissues, and significant correlation between IL18 promoter methylation and increased infiltration of CD8+ T cells[32]. Additionally, some studies have found that IL18 inhibits T cell activity and accelerates multiple myeloma[33]. IL18 has become a key player and research hotspot in the progression of different types of tumors. Studying its potential role in the pathogenesis of gliomas and demonstrating its utility as a potential biomarker for LGG is meaningful.

Tumor-associated macrophages (TAMs) play a crucial role in the occurrence and development of human cancers. As an integral part of the tumor microenvironment, TAMs influence tumor progression, angiogenesis, and immune regulation[34]. Wang et al. found that increased TAMs may be an immune evasion mechanism in gliomas, and TAM-related features could provide therapeutic targets for gliomas[35]. Fang et al. discovered that the tumor microenvironment plays a vital role in the occurrence, development, and treatment of gliomas, with glioma-associated macrophages (GAMs) being the main cell population involved in immune function[36]. In this study, we found that the StromalScore, ImmuneScore, and EstimateScore of the IL18 high-expression group were higher than those of the low-expression group, and the infiltration of M2 macrophages was significantly increased in the IL18 high-expression group. In LGG patients, IL18 scores were negatively correlated with immune therapy response. Therefore, IL18, as a potential therapeutic target, holds great promise.

With the rapid development of medical imaging technologies such as computed tomography (CT), magnetic resonance imaging (MRI), positron emission tomography (PET), and ultrasound (US), medical imaging plays a more central role in personalized medicine[37,38]. Radiomics extracts and analyzes medical imaging data through data collection, tumor segmentation, feature extraction, and model establishment, combined with clinical information, to improve the accuracy of diagnosis and treatment response[39–41]. Kamel et al. predicted the histological differentiation of hepatocellular carcinoma tissue using MRI radiomics features[42]. Bai et al. predicted the classification of pancreatic cystic tumors using radiomics models[43]. Tian et al. confirmed the relationship between CT radiomics features and overall survival in patients with non-small cell lung cancer (NSCLC), providing clinical value for guiding personalized treatment plan selection for NSCLC[44]. Compared to detection of peripheral blood samples, fresh tissue specimens, or paraffin-embedded tissue specimens, radiomics can be applied preoperatively for tumor diagnosis, prediction of tumor staging, and treatment efficiency, which will save medical resources, reduce medical costs, and alleviate patient suffering[45]. In this study, we randomly divided the screened TCIA data into training and validation sets to build models, and used single-center data as an external dataset to validate the model. The AUC values of the training set, validation set, and external validation set were 0.861, 0.788, and 0.762, respectively. The calibration curve showed that the model had good predictive performance, and decision curve analysis (DCA) showed that the model had high clinical utility. In the validation set, training set, and external test set, higher expression of IL18 was associated with higher Rad_score values. Kaplan-Meier survival curves showed a significant correlation between high Rad_score and worse overall survival (OS), suggesting that the model has good efficiency in predicting IL18 expression and clinical prognosis. With the rapid development of

Table 2 | The data set is divided into training set and validation set

Variables	Total (n = 139)	Train (n = 98)	Validation (n = 41)	p
IL18, n (%)				1
Low	90 (65)	63 (64)	27 (66)	
High	49 (35)	35 (36)	14 (34)	
Age, n (%)				0.734
~40	59 (42)	43 (44)	16 (39)	
41~	80 (58)	55 (56)	25 (61)	
Gender, n (%)				0.869
Female	71 (51)	51 (52)	20 (49)	
Male	68 (49)	47 (48)	21 (51)	
Histologic_grade, n (%)				0.836
G2	71 (51)	49 (50)	22 (54)	
G3	68 (49)	49 (50)	19 (46)	
Radiotherapy, n (%)				1
NO	46 (33)	32 (33)	14 (34)	
YES	93 (67)	66 (67)	27 (66)	
Histological_type, n (%)				0.53
Astrocytoma	46 (33)	35 (36)	11 (27)	
Oligoastrocytoma	34 (24)	22 (22)	12 (29)	
Oligodendroglioma	59 (42)	41 (42)	18 (44)	
Chr_1p_19q_codeletion, n (%)				0.476
Codel	38 (27)	29 (30)	9 (22)	
Non-Codel	101 (73)	69 (70)	32 (78)	
IDH_status, n (%)				1
Mutant	109 (78)	77 (79)	32 (78)	
WT	30 (22)	21 (21)	9 (22)	
MGMT_promoter_status, n (%)				0.725
Methylated	111 (80)	77 (79)	34 (83)	
Unmethylated	28 (20)	21 (21)	7 (17)	
Chemotherapy, n (%)				1
NO	45 (32)	32 (33)	13 (32)	
YES	94 (68)	66 (67)	28 (68)	
OS, n (%)				0.504
Alive	102 (73)	74 (76)	28 (68)	
Dead	37 (27)	24 (24)	13 (32)	
OS. time, Median (Q1, Q3)	21.7 (14.97, 40.7)	20.27 (14.39, 38.57)	30.27 (17.77, 48.97)	0.036

science and technology, artificial intelligence (AI) and machine learning (ML) have promoted the efficiency and precision of tumor screening, diagnosis, and treatment[46]. AI and ML technologies can analyze large amounts of medical imaging data and pathological diagnosis results, construct different models through methods such as image segmentation and feature extraction, and evaluate the efficacy of different treatment regimens. This not only helps doctors more accurately judge the condition but also provides decision-making basis for doctors[47]. In recent years, IL18 has shown great potential in the treatment of various types of tumors, and numerous studies are exploring IL18-targeted tumor therapies[30–32]. Recent research indicates that small molecule drugs targeting IL18 have demonstrated good efficacy in tumor treatment and show great application prospects[11]. Unfortunately, current IL18 detection methods are typically invasive, expensive, and based on local tumor tissue, which not only fails to represent the overall tumor condition but also makes dynamic observation difficult. Therefore, this study constructed a noninvasive radiomics prediction model for IL18 based on the LGG, capable of predicting patient prognosis. The noninvasive prediction model provides new indicators for personalized precision treatment, enables dynamic monitoring of IL18, and lays the foundation for predicting IL18-related therapies. In the future, it can also be used to screen populations potentially benefiting from IL18-targeted therapy.

The main limitation of this study is the use of only a single-center external dataset for validation, with a relatively small sample size, which may introduce potential selection bias. To improve the model's stability and generalizability, a multi-sequence fusion approach could be implemented, with subsequent validation using large-scale, multi-center datasets that encompass broader population demographics and increased sample sizes. We will further explore this in future research.

Methods

Patient data

This study obtained transcriptome sequencing data, imaging data, and complete corresponding clinical information of patients with low-grade gliomas (LGG) from The Cancer Genome Atlas (TCGA) (https://portal.gdc.cancer.gov/) and The Cancer Imaging Archive

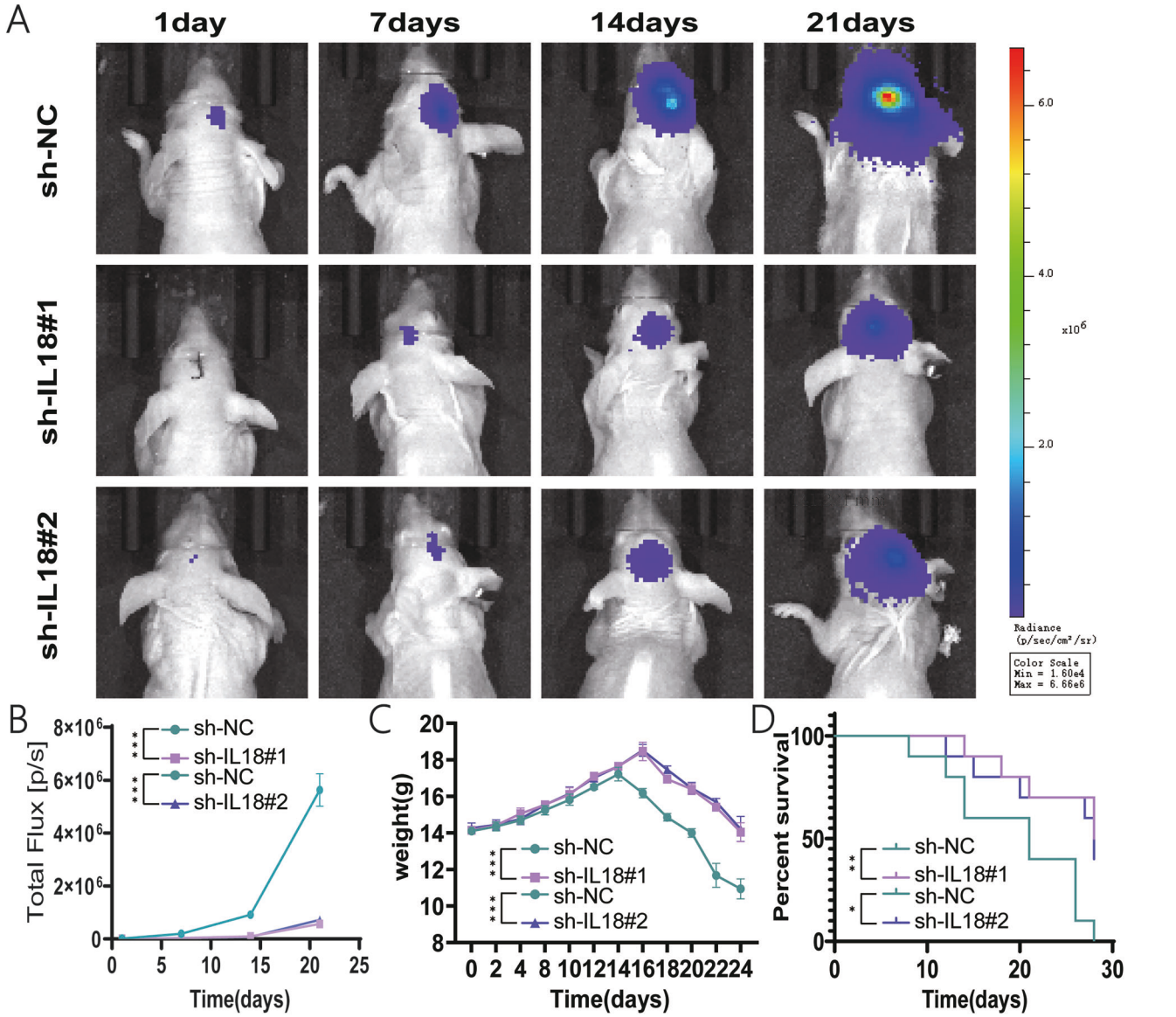

Fig. 5 | Knockout of IL18 can inhibit the growth of glioma in vivo. In vivo imaging was used to assess the fluorescence intensity of intracranial tumors in nude mice on days 1, 7, 14, and 21 (**A**) and statistical analysis (**B**). Body weight (**C**) and survival analysis (**D**) of nude mice were conducted at different time points (*$p < 0.05$, **$p < 0.01$, ***$p < 0.001$).

(TCIA) (https://www.cancerimagingarchive.net/) databases. The inclusion criteria were patients classified as WHO Grade II or III with complete prognosis information. Finally, clinical and RNA-seq data from TCGA-LGG (n = 461) and enhanced MRI (enhanced T1WI, n = 139) from TCIA-LGG were obtained to explore the prognostic value of IL18, construct radiomics prediction models, and investigate the prognostic value of the model. This study collected imaging data and corresponding clinical information of 50 patients with low-grade gliomas who were treated at the Second Affiliated Hospital of Nanchang University from 2020 to 2023 as an external validation set. Informed consent was obtained from all participants prior to their involvement in the study. The study was conducted in accordance with the Declaration of Helsinki. This study was approved by the Ethics Review Committee of the Second Affiliated Hospital of Nanchang University, China (Project approval ID: O-Medical Research Ethics Review (2024) (No.21).

IL18 expression-related analysis

RNAseq data and corresponding clinical information from the TCGA_GBM, TCGA_LGG, and CGGA_325 projects were downloaded and organized from the TCGA database (https://portal.gdc.cancer.gov) and CGGA database (https://www.cgga.org.cn/). The TCGA_GBM and CGGA_325 datasets were used exclusively for analyzing the involvement of IL18 in the malignant progression of gliomas. The cutoff value was determined using the "survminer" R package[48,49]. Differential analysis, survival analysis, univariate, and multivariate Cox regression analysis were performed using the "limma," "survival," and "forestplot" R packages to explore the impact factors of OS and the effects of multiple influencing factors. Exploratory subgroup analysis was conducted through univariate Cox regression to analyze the impact of IL18 high and low expression groups on patient prognosis in different subgroups of each covariate[50]. Spearman rank correlation coefficient was used to analyze the correlation between IL18 and tumor clinical features, and the correlation heatmap was displayed.

RNA isolation and qRT-PCR

Samples of 16 patients with low-grade glioma treated at the Second Affiliated Hospital of Nanchang University Neurosurgery Department from 2020 to 2023, and six samples of normal brain tissue were collected to detect the expression status of IL18. Total RNA was extracted from the tissue using

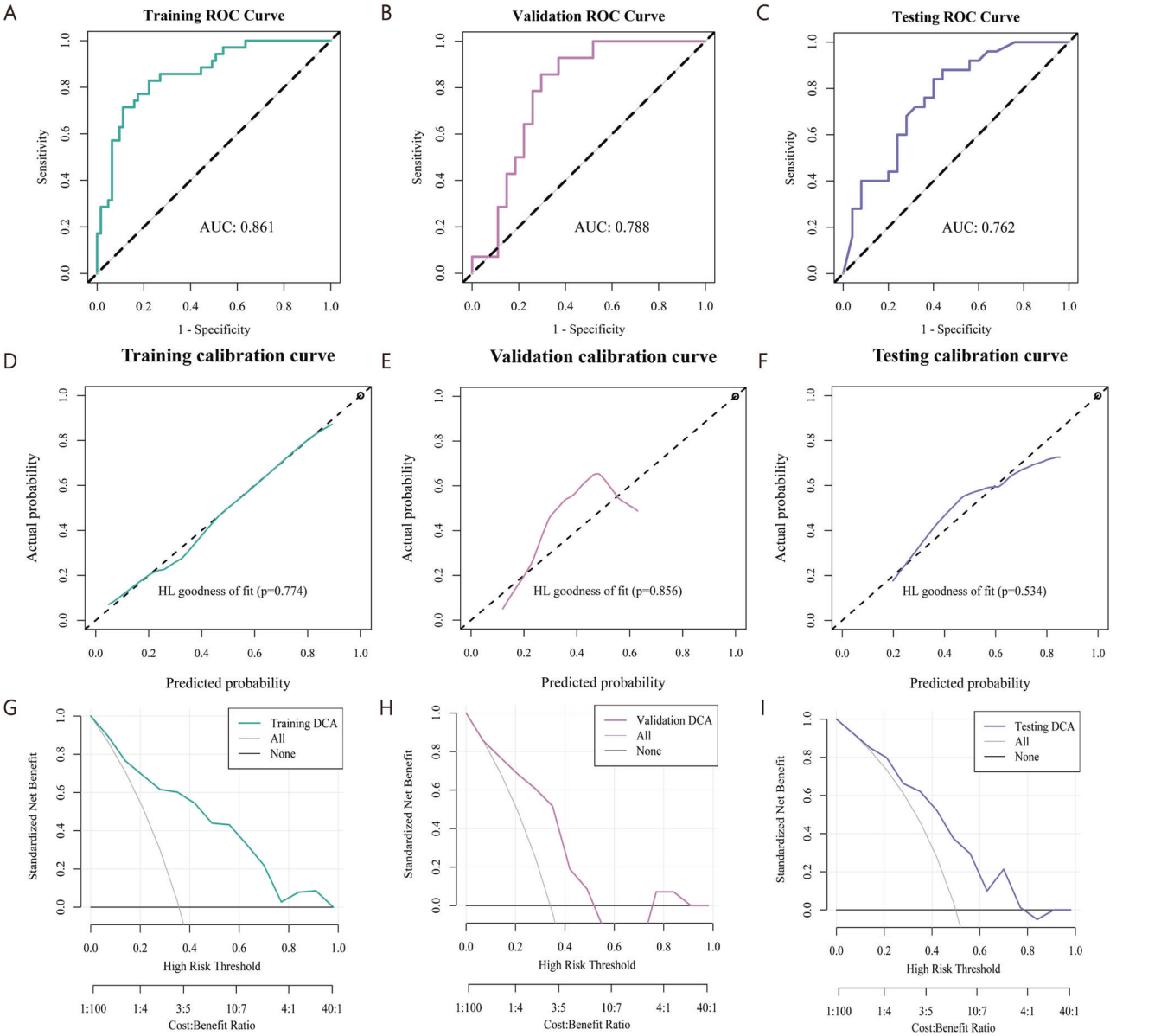

Fig. 6 | Construction and evaluation of radiomics model. Analysis of the constructed radiomics model ROC curve in the training set (**A**), validation set (**B**), and external test set (**C**); Calibration curve analysis in the training set (**D**), validation set (**E**), and external test set (**F**); Decision curve analysis (DCA) in the training set (**G**), validation set (**H**), and external test set (**I**).

Simply P Total RNA Extraction (BioFluX, Shiga, BSC52M1). Reverse transcription was performed using MonScript RTII All-in-One Mix with dsDNase (Monad, MRO5101T), and the quantity of isolated RNA was measured using the MonAmp RapidStart Universal SYBR Green qPCR Mix (Monad, MQ10701S). The primer for IL18 was forward 5′-TCTTCATTGACCAAGGAAATCGG-3′and reverse 5′-TCCGGGGTGCATTATCTCTAC-3′.

Immunohistochemistry (IHC)

Samples of 50 patients with low-grade glioma treated at the Second Affiliated Hospital of Nanchang University Neurosurgery Department from 2020 to 2023, and six samples of normal brain tissue were collected to detect the expression status of IL18 using the IHC method. Firstly, the tissue samples were fixed with fixative and embedded in paraffin blocks for slide preparation. The 5 μm-thick glioma tissue sections were deparaffinized in xylene, dehydrated through a series of decreasing ethanol concentrations followed by rehydration, and washed in distilled water. Subsequently, the sections were fully immersed in 3% hydrogen peroxide solution at room temperature, followed by incubation for 10 min and rinsing in running water for 5 min. Finally, staining, dehydration, clearing, and mounting were performed using IL18 Rabbit mAb (ABclonal, A23076) according to the manufacturer's instructions. The most appropriate dilution concentration selected was 1:500. The IHC results were evaluated by two senior pathologists independently under a microscope at ×10 and ×20 magnification.

Enrichment analysis

Gene Set Variation Analysis (GSVA) can calculate the enrichment score of a specific gene set in each sample[51]. The pathway enrich score of KEGG pathway gene sets and Hallmark gene sets in each sample was calculated using the "GSVA" R package, and the top 50 pathways were visualized respectively.

Single-cell sequencing analysis

The scTIME Portal was used to obtain and analyze the expression of IL18 in different cell components of the GSE138794 glioma data set[52].

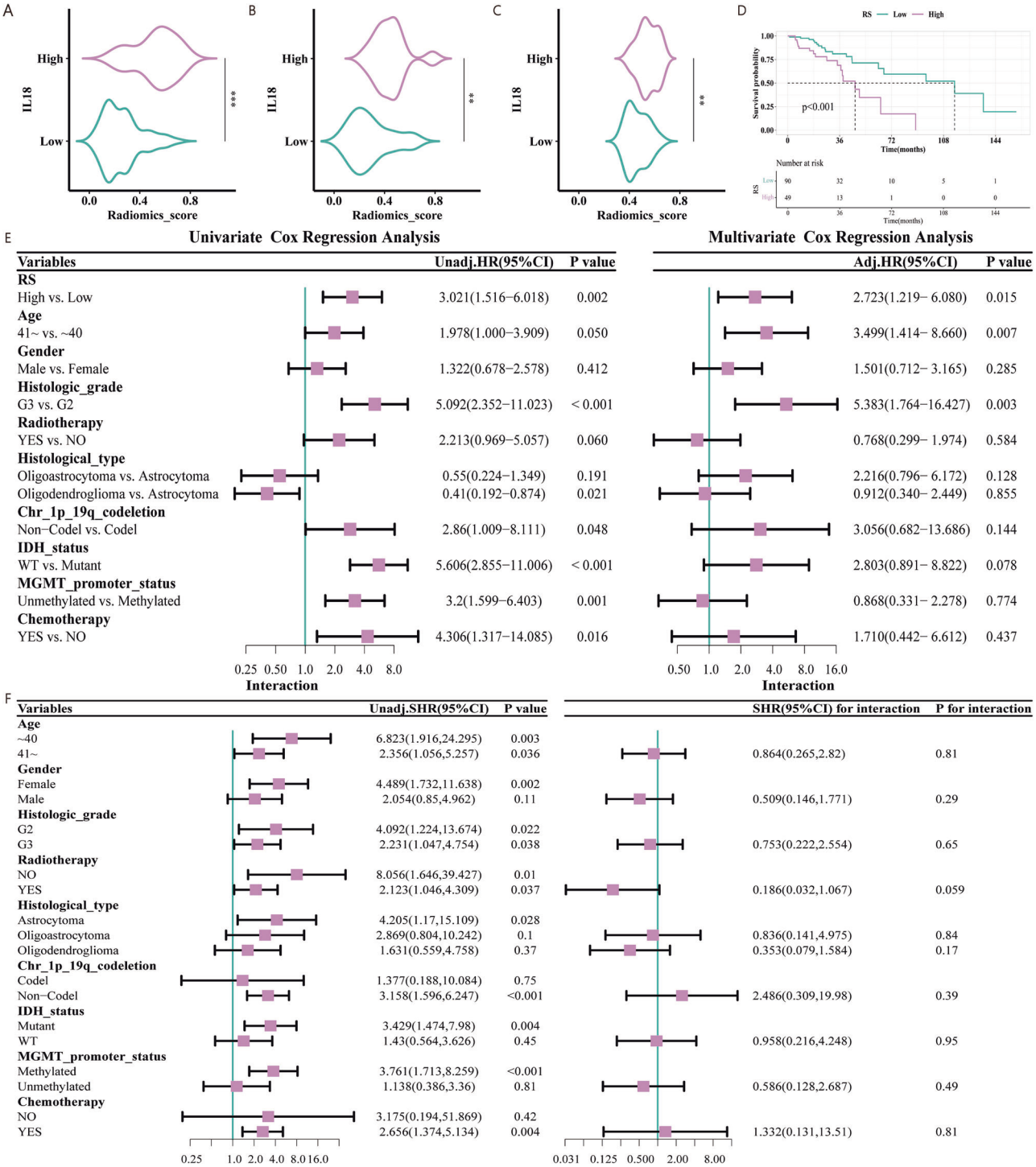

Fig. 7 | Relationship between radiomics score and clinical features. Correlation between RS and IL18 expression in the training set (**A**), validation set (**B**), and external test set (**C**). **D** Kaplan-Meier curve shows a significant correlation between high expression of RS and deteriorated OS; **E** Univariate and multivariate Cox regression analyses show that Rad_score is an independent prognostic factor for OS; **F** Impact of Rad_score on patient prognosis in various subgroups through subgroup analysis. (*p < 0.05, **p < 0.01, ***p < 0.001).

Tumor microenvironment analysis and immune cell infiltration analysis

Analysis of Tumor Microenvironment and Immune Cell Infiltration Immunoscore, stromal score, and estimate score representing the tumor microenvironment (TME) were calculated in TCGA-LGG samples using the "estimate" R package[53]. Low-grade glioma samples were uploaded to the CIBERSORTx database (https://cibersortx.stanford.edu/) to compute immune cell infiltration and analyze the degree of immune cell infiltration between IL18 high and low expression groups. Low-grade glioma samples were also uploaded to the TIDE database (http://tide.dfci.harvard.edu) to evaluate the response of immune checkpoint inhibitors (ICI) using the Tumor Immune Dysfunction and Exclusion (TIDE) algorithm[54].

Cell culture and transfection

The glioma cell lines U118MG and U251MG were obtained from the American Type Culture Collection (ATCC, USA) and cultured in DMEM

(Dulbecco's Modified Eagle Medium) supplemented with 10% fetal bovine serum. The glioma cells were transfected with lentiviral vectors containing IL18 shRNA#1 (5'-GGCCTCTATTTGAAGATATGA-3'), IL18 shRNA#2 (5'-GGAAATGAATCCTCCTGATAA-3'), and a negative control (NC).

Colony formation assay, wound healing assay, transwell assay

Cells after transfection were cultured in 6-well plates (1000 cells/well) for two weeks. Colonies were stained with 0.1% crystal violet for observation and manual counting. When the transfected cells reached 85% confluence in the 6-well plates, a wound was created by scratching with a sterile 10 μl pipette tip. Photographs of the wound were captured at two different time intervals (0 and 24 h). In the invasion assay, transfected cells were resuspended in serum-free medium according to the manufacturer's instructions. A total of 5 × 10^4 cells were seeded into the upper chamber of a 24-well plate (Corning, USA). The membrane of the upper chamber was pre-coated with Matrigel (Yeasen, China) diluted 1:8. In the lower chamber, 500 μL of medium supplemented with 25% fetal bovine serum was added. After incubating at 37 °C for 24–48 h, invaded cells were observed under a microscope.

Nude mouse in vivo tumor model

Four-week-old female BALB/c nude mice were purchased from the Experimental Animal Center of Nanjing Medical University. U251-sh-NC, U251-sh-IL18#1, and U251-sh-IL18#2 cells (5 × 10^5 cells) were implanted into the brains of nude mice using a stereotactic apparatus (RWD Life Science, Shenzhen, China) to establish an intracranial tumor model (n = 5 per group). The formation of intracranial tumors and assessment of tumor size were confirmed on days 1, 7, 14, and 21 using the IVIS Spectrum real-time imaging system (Branford, USA), and corresponding body weight changes were recorded. This study was approved by the Ethics Committee for Experimental Animals of Nanchang University (No. NCULAE-20221031035).

MRI imaging parameters and image preprocessing

Specific parameters of MRI imaging: Manufacturer(GE MEDICAL SYSTEMS, General Electric, Philips Medical Systems, SIEMENS, HITACHI MEDICAL CORPORATION.) Min-max: median. Slice Thickness: 1–5; 2. Spacing Between Slices: 1–7.5; 2.5. Pixel_Spacings: 0.391–1.016; 0.75. Repetition Time: 4.616–3236.34; 500. Echo Time: 1.69–20; 4.6.

The image preprocessing process includes: (i) N4 Bias Field Correction: Applied to reduce signal deviations caused by magnetic field inhomogeneity, thereby improving image consistency. (ii) Resampling to [1,1,1] mm^3: Ensures isotropic voxel dimensions, aligning pixel distributions across images from different sources and reducing variations in spatial resolution caused by differences in scanning equipment. (iii) Normalization (normalizeScale = 100): Reduced differences in pixel value distributions across devices, enhancing feature comparability. (iv) Discretization (binWidth = 5): Minimized the influence of pixel noise, stabilizing feature calculations.

Radiomic feature extraction and model construction

Segmentation was performed using 3D Slicer software (version 4.10.2; https://www.slicer.org/). Two radiologists, each with 15 years of experience in radiology, independently manually contoured the lesions layer by layer without knowledge of the patients' clinical data and diagnostic results. "PyRadiomics" R package was used to resampling images to make them isotropic, so as to reduce the variation caused by differences in scanning equipment and protocols and different lesion sizes of patients. Then image standardization is used to reduce image noise and standardize the intensity, reducing the difference in the intensity of the image signal acquired by different machines. Finally, 107 original radiomics features, including shape, first-order, and second-order features, were extracted using "PyRadiomics" R package. The dataset was randomly divided into training and validation sets in a 7:3 ratio using the "caret" and "CBCgrps" R packages, and differential analysis was conducted between the two groups. Radiomic features were extracted from the TCGA-TCIA intersection samples (n = 139) using the "PyRadiomics" R package. The consistency of extracted radiomic features was evaluated using the Intraclass Correlation Coefficient (ICC), with a median ICC value of 0.955 and 103 radiomic features having ICC values ≥0.75. Further feature selection was performed using the Maximum Relevance Minimum Redundancy (mRMR) and Recursive Feature Elimination (RFE) methods. The selected radiomic features were then used to model gene expression using the Gradient Boosting Machine algorithm for prediction.

Evaluation of radiomics model and analysis of radiomics score correlation

The ROC curve refers to the receiver operating characteristic curve, which is a comprehensive index reflecting the sensitivity and specificity of continuous variables. The diagnostic efficiency is evaluated by calculating the area under the ROC–AUC curve[55]. The calibration of the predictive model was evaluated using calibration curves and the Hosmer-Lemeshow goodness-of-fit test. The overall performance of the radiomics model was quantified using the Brier score, which yielded values of 0.151 and 0.184 for the training and validation sets, respectively. The decision curve analysis (DCA) was employed to assess the clinical utility of the radiomics prediction model[56]. The Radiomics score (Rad_score), which outputs the probability of predicting gene expression levels, was determined using the "survminer" R package to determine the cutoff value and divide into high-expression and low-expression groups.

Statistical analysis

Categorical variables were expressed as frequencies and percentages (%), and Fisher's exact test or chi-square test was used to compare clinical characteristics[57]. Non-normally distributed continuous variables were compared between groups using the Wilcoxon test[58]. The Log-rank test was used to assess the significance of survival rates between groups, with median survival time defined as the survival time corresponding to a 50% survival rate[59]. The "CBCgrps" package in R language was used for baseline comparison, "Survival", "cmprsk", and "forestplot" packages for survival analysis and visualization, and "clusterProfiler" and "stats" packages for exploring the biological mechanisms of radiomics features and diseases. All analyses were conducted using R software version 4.1.0, with two-sided tests and a significance level of $P < 0.05$ indicating a significant difference.

Data availability

The TCGA glioma data used to support the analysis in this study were downloaded from TCGA (http://portal.gdc.cancer.gov). The glioma imaging data were obtained from TCIA (https://www.cancerimagingarchive.net/). The CGGA glioma data used in this study to support the analysis can be downloaded from CGGA (http://www.cgga.org.cn/). Contact the corresponding author via email for requests.

Code availability

Contact the corresponding author via email for requests.

Received: 24 November 2024; Accepted: 27 May 2025;
Published online: 19 June 2025

References

1. Sung, H. et al. Global Cancer Statistics 2020: GLOBOCAN estimates of incidence and mortality worldwide for 36 cancers in 185 countries. *CA Cancer J. Clin.* **71**, 209–249 (2021).
2. Franceschi, E. et al. Rare primary central nervous system tumors in adults: an overview. *Front. Oncol.* **10**, 996 (2020).
3. Louis, D. N. et al. The 2016 World Health Organization classification of tumors of the central nervous system: a summary. *Acta Neuropathol.* **131**, 803–820 (2016).
4. Diaz, M., Jo, J., Smolkin, M., Ratcliffe, S. J. & Schiff, D. Risk of venous thromboembolism in grade II-IV gliomas as a function of molecular subtype. *Neurology* **96**, e1063–e1069 (2021).

5. Weller, M. et al. European Association for Neuro-Oncology (EANO) guideline on the diagnosis and treatment of adult astrocytic and oligodendroglial gliomas. *Lancet Oncol.* **18**, e315–e329 (2017).
6. Garlanda, C., Dinarello, C. A. & Mantovani, A. The interleukin-1 family: back to the future. *Immunity* **39**, 1003–1018 (2013).
7. Mantovani, A., Dinarello, C. A., Molgora, M. & Garlanda, C. Interleukin-1 and related cytokines in the regulation of inflammation and immunity. *Immunity* **50**, 778–795 (2019).
8. Nakanishi, K., Yoshimoto, T., Tsutsui, H. & Okamura, H. Interleukin-18 regulates both Th1 and Th2 responses. *Annu. Rev. Immunol.* **19**, 423–474 (2001).
9. Nakanishi, K. Unique action of Interleukin-18 on T cells and other immune cells. *Front. Immunol.* **9**, 763 (2018).
10. Yasuda, K., Nakanishi, K. & Tsutsui, H. Interleukin-18 in health and disease. *Int. J. Mol. Sci.* **20**, 649 (2019).
11. Zhou, T. et al. IL-18BP is a secreted immune checkpoint and barrier to IL-18 immunotherapy. *Nature* **583**, 609–614 (2020).
12. Simpson, S., Kaislasuo, J., Guller, S. & Pal, L. Thermal stability of cytokines: a review. *Cytokine* **125**, 154829 (2020).
13. Zhang, J. et al. Triazoles as T(2)-exchange Magnetic Resonance Imaging contrast agents for the detection of Nitrilase activity. *Chemistry* **24**, 15013–15018 (2018).
14. Cai, X. et al. N-Aryl Amides as chemical exchange saturation transfer Magnetic Resonance Imaging contrast agents. *Chemistry* **26**, 11705–11709 (2020).
15. Makanyanga, J. et al. MRI texture analysis (MRTA) of T2-weighted images in Crohn's disease may provide information on histological and MRI disease activity in patients undergoing ileal resection. *Eur. Radiol.* **27**, 589–597 (2017).
16. Li, M. et al. Computed tomography texture analysis to facilitate therapeutic decision making in hepatocellular carcinoma. *Oncotarget* **7**, 13248–13259 (2016).
17. Korenchan, D. E. et al. (31)P spin-lattice and singlet order relaxation mechanisms in pyrophosphate studied by isotopic substitution, field shuttling NMR, and molecular dynamics simulation. *Phys. Chem. Chem. Phys.* **24**, 24238–24245 (2022).
18. Li, Z. et al. Texture-based classification of different single liver lesion based on SPAIR T2W MRI images. *BMC Med. imaging* **17**, 42 (2017).
19. Park, J. E. et al. Radiomics prognostication model in glioblastoma using diffusion- and perfusion-weighted MRI. *Sci. Rep.* **10**, 4250 (2020).
20. Choi, Y. S. et al. Incremental prognostic value of ADC histogram analysis over MGMT promoter methylation status in patients with glioblastoma. *Radiology* **281**, 175–184 (2016).
21. Kesari, S. et al. Phase II study of protracted daily temozolomide for low-grade gliomas in adults. *J. Am. Assoc. Cancer Res.* **15**, 330–337 (2009).
22. Claus, E. B. & Verhaak, R. G. W. Targeting IDH in low-grade glioma. *N. Engl. J. Med.* **389**, 655–659 (2023).
23. Leu, S., von Felten, S., Frank, S., Boulay, J. L. & Mariani, L. IDH mutation is associated with higher risk of malignant transformation in low-grade glioma. *J. Neuro-Oncol.* **127**, 363–372 (2016).
24. Kinslow, C. J. et al. Association of MGMT promoter methylation with survival in low-grade and anaplastic gliomas after alkylating chemotherapy. *JAMA Oncol.* **9**, 919–927 (2023).
25. Everhard, S. et al. MGMT methylation: a marker of response to temozolomide in low-grade gliomas. *Ann. Neurol.* **60**, 740–743 (2006).
26. Liu, S. et al. NK cell-based cancer immunotherapy: from basic biology to clinical development. *J. Hematol. Oncol.* **14**, 7 (2021).
27. Chapman, N. M., Boothby, M. R. & Chi, H. Metabolic coordination of T cell quiescence and activation. *Nat. Rev. Immunol.* **20**, 55–70 (2020).
28. Berg, R. E., Cordes, C. J. & Forman, J. Contribution of CD8+ T cells to innate immunity: IFN-gamma secretion induced by IL-12 and IL-18. *Eur. J. Immunol.* **32**, 2807–2816 (2002).
29. Freeman, C. M. et al. Cytotoxic potential of lung CD8(+) T cells increases with chronic obstructive pulmonary disease severity and with in vitro stimulation by IL-18 or IL-15. *J. Immunol.***184**, 6504–6513 (2010).
30. Deswaerte, V. et al. Inflammasome adaptor ASC suppresses apoptosis of gastric cancer cells by an IL18-mediated inflammation-independent mechanism. *Cancer Res.* **78**, 1293–1307 (2018).
31. Jarry, A. et al. Role of the inflammasome of tumor cells in modulating the biology of Tumor Infiltrating Lymphocytes (TILs) in colorectal cancer. *J. Clin. Oncol.* **35**, e23087-e23087 (2017).
32. Wang, X. et al. The prognostic value and immune correlation of IL18 expression and promoter methylation in renal cell carcinoma. *Clin. Epigenet.***15**, 14 (2023).
33. American Association for Cancer Research. IL18 promotes MDSC-mediated immunosuppression in multiple myeloma. *Cancer Discov.* **8**, OF12-OF12 (2018).
34. Bied, M., Ho, W. W., Ginhoux, F. & Blériot, C. Roles of macrophages in tumor development: a spatiotemporal perspective. *Cell. Mol. Immunol.* **20**, 983–992 (2023).
35. Wang, L. J., Xue, Y. & Lou, Y. Tumor-associated macrophages related signature in glioma. *Aging* **14**, 2720–2735 (2022).
36. Xu, C. et al. Origin, activation, and targeted therapy of glioma-associated macrophages. *Front. Immunol.* **13**, 974996 (2022).
37. Lambin, P. et al. Radiomics: extracting more information from medical images using advanced feature analysis. *Eur. J. Cancer* **48**, 441–446 (2012).
38. Lambin, P. et al. Radiomics: the bridge between medical imaging and personalized medicine. *Nat. Rev. Clin. Oncol.* **14**, 749–762 (2017).
39. Kumar, V. et al. Radiomics: the process and the challenges. *Magn. Reson. Imaging* **30**, 1234–1248 (2012).
40. Gillies, R. J., Kinahan, P. E. & Hricak, H. Radiomics: images are more than pictures, they are data. *Radiology* **278**, 563–577 (2016).
41. Rios Velazquez, E. et al. Somatic mutations drive distinct imaging phenotypes in lung cancer. *Cancer Res.* **77**, 3922–3930 (2017).
42. Ameli, S. et al. Role of MRI-derived radiomics features in determining degree of tumor differentiation of hepatocellular carcinoma. *Diagnostics***12**, 2386 (2022).
43. Liang, W. et al. Classification prediction of pancreatic cystic neoplasms based on radiomics deep learning models. *BMC Cancer* **22**, 1237 (2022).
44. Song, J. et al. Non-small cell lung cancer: quantitative phenotypic analysis of CT images as a potential marker of prognosis. *Sci. Rep.* **6**, 38282 (2016).
45. Liu, Z. et al. The applications of radiomics in precision diagnosis and treatment of oncology: opportunities and challenges. *Theranostics* **9**, 1303–1322 (2019).
46. Petrick, L. M. & Shomron, N. AI/ML-driven advances in untargeted metabolomics and exposomics for biomedical applications. *Cell Rep. Phys. Sci.* **3**, 100978 (2022).
47. Toh, T. S., Dondelinger, F. & Wang, D. Looking beyond the hype: applied AI and machine learning in translational medicine. *EBioMedicine* **47**, 607–615 (2019).
48. Yu, Y. et al. Development and validation of a preoperative magnetic resonance imaging radiomics-based signature to predict axillary lymph node metastasis and disease-free survival in patients with early-stage breast cancer. *JAMA Netw. Open* **3**, e2028086 (2020).
49. Lv, L. et al. Radiomic analysis for predicting prognosis of colorectal cancer from preoperative (18)F-FDG PET/CT. *J. Transl. Med.* **20**, 66 (2022).
50. Amatya, A. K. et al. Subgroup analyses in oncology trials: regulatory considerations and case examples. *J. Am. Assoc. Cancer Res.* **27**, 5753–5756 (2021).
51. Hänzelmann, S., Castelo, R. & Guinney, J. GSVA: gene set variation analysis for microarray and RNA-seq data. *BMC Bioinform.* **14**, 7 (2013).

52. Hong, F. et al. Single-cell analysis of the pan-cancer immune microenvironment and scTIME portal. *Cancer Immunol. Res.* **9**, 939–951 (2021).
53. Yoshihara, K. et al. Inferring tumour purity and stromal and immune cell admixture from expression data. *Nat. Commun.* **4**, 2612 (2013).
54. Jiang, P. et al. Signatures of T cell dysfunction and exclusion predict cancer immunotherapy response. *Nat. Med.* **24**, 1550–1558 (2018).
55. Mandrekar, J. N. Receiver operating characteristic curve in diagnostic test assessment. *J. Thorac. Oncol.***5**, 1315–1316 (2010).
56. Zhang, L. et al. Multicenter clinical radiomics-integrated model based on [(18)F]FDG PET and multi-modal MRI predict ATRX mutation status in IDH-mutant lower-grade gliomas. *Eur. Radiol.* **33**, 872–883 (2023).
57. Jung, S. H. Stratified Fisher's exact test and its sample size calculation. *Biom. J.* **56**, 129–140 (2014).
58. Ballenberger, N., Lluis, A., von Mutius, E., Illi, S. & Schaub, B. Novel statistical approaches for non-normal censored immunological data: analysis of cytokine and gene expression data. *PloS ONE* **7**, e46423 (2012).
59. Seiler, R. et al. Impact of molecular subtypes in muscle-invasive bladder cancer on predicting response and survival after neoadjuvant chemotherapy. *Eur. Urol.* **72**, 544–554 (2017).

Acknowledgements

This study was supported by the National Natural Science Foundation of China (No. 82360544), Jiangxi Provincial Natural Science Foundation (No.20232ACB206045), Health Commission of Jiangxi Province (No. 202130356), Education Department of Jiangxi Province (No. GJJ200178). The funder, HG, contributed to the conceptualization and experimental design, and played a role in the preparation of the manuscript.

Author contributions

Z.Z., Y.X., and J.L. contributed equally to this work. The experiments were conceived and designed by Z.Z., Y.X., and H.G. Experimental data were downloaded and analyzed by J.L. and F.X. J.Z. and W.T. were used for image sketch analysis. The manuscript was written by Z.Z., H.Z., and H.G. All authors read and approved the final manuscript.

Competing interests

The authors declare no competing interests.

Additional information

Supplementary information The online version contains supplementary material available at https://doi.org/10.1038/s41698-025-00966-x.

Correspondence and requests for materials should be addressed to Hong Zhu, Wei Tu or Hua Guo.